Multi-port converter for medium and high voltage applications

F. Alsokhiry and Y. Al-Turki
King Abdulaziz University,
Jeddah, Kingdom of Saudi Arabia

Ibrahim Abdelsalam
Arab Academy for Science and Technology and Maritime Transport, Cairo, Egypt

G.P. Adam and K.H. Ahmed
University of Strathclyde
grain.adam@strath.ac.uk

***Abstract*—This work presents a multi-port converter (MPC) that is well-suited for use as a hybrid hub in complex multi-terminal high-voltage direct current (MTDC) networks. The proposed MPC generates several and controllable DC voltages from a constant or variable input DC voltage or AC grid. Its operating principle is explained and corroborated using simulations and experimentations.**

***Key words*—DC-DC converters for future DC grids; hybrid DC-DC and DC-AC hubs; DC power and voltage control, and auto DC transformers**

I. Introduction

MTDC grids represent the initial step for realisation of future super grids to facilitate bulky powers transfer over long distances, with tight control over the directions and magnitudes of the power transfer in each DC line[1-7]. Such MTDC systems are anticipated to consist of more than one DC voltage levels[8-13]. The DC voltage magnitude of each section will be dictated by the magnitude of power to be transferred and DC cables ratings. In MTDC grids, DC transformers are anticipated to play important roles such as DC voltage and power control, and definition of protection zones, where galvanic isolation and DC fault containment are essential[14-16].

In recent years, a number of isolated and non-isolated DC transformers were suggested for possible use in MTDC grids [17-20]. Most of the existing isolated DC transformers have adopted the basic circuit structure of the dual active bridge (DAB) or front-to-front (F2F) connected AC/DC converters. These DC transformers capable of stopping propagation of DC fault outside the faulted DC side. Such attribute could be utilized to decrease the amount of DC circuit breakers and to split large MTDC grids into a number of self-contained isolated DC networks. The major weakness of the F2F DC transformers is that the HV and LV converters and isolation AC transformer are sized for full power, and this decreases their efficiencies.

In an attempt to decrease the cost, size and weight of the F2F DC transformers, the work in [21] operates the MMC based DC transformer in a quasi-two-level (Q2L) mode. This work has shown that the Q2L-MMC based DC transformer exposes the isolating transformer to a low and controllable *dv/dt*. Also, it reduces the submodule capacitance, arm inductance and current rating of the semiconductor switches of the half-bridge submodule (HB-SM), particularly, the switches that insert the sub-modules' capacitors into the power path.

Further reduction in the capital cost and footprint of MMC based F2F DC transformer is achieved through adoption of the transition arm converter (TAC)[22].

Many works have promoted the non-isolated F2F DC transformers as alternative to isolated version, particularly, to reduce cost, weight and losses. Although the non-isolated DC transformer can contain the impact of pole-to-pole DC short circuit faults within the faulty side, it is unable to contain the impact of pole-to-ground, particularly, the substantial shift of the insulation level of the healthy pole.

The most promising partially isolated DC transformer with circuit structure resembles auto transformer was proposed in [19]. Its main attributes are: the rated power could be exchanged between the HV and LV sides, and the same time the semiconductor switches of the LV side and isolation transformer that connects upper and lower sub-converters (SC_1 and SC_2) are fractionally rated. Numerous variations of this auto DC transformer are discussed in [19]. Nonetheless, the immense potentials exist in the DC transformers in [19] are not fully exploited. From DC fault ride-through viewpoint, the asymmetric monopole nature of SC_1 and SC_2 makes the DC transformer in in [19] to DC faults; especially, as any DC fault that may occur in its DC side resembles pole-to-pole DC short-circuit fault. For examples, a pole-to-ground DC fault in the positive pole creates a short circuit fault across SC_1, while a pole-to-ground DC fault in the negative pole creates a short circuit fault across SC_2.

In [17], numerous non-isolated buck and boost hybrid cascaded DC transformers are proposed for HVDC applications. In these DC transformers, the FB cells in each limb are used to filter-out the deliberately injected AC components in order to generate any desired DC voltage magnitude from a fixed input DC voltage. The absence of AC transformers in the hybrid cascaded DC transformers in [17] is advantageous as this leads to cheaper and lighter DC transformers than those presented in [19]. However, the major deficiency of these topologies is that the series connected switches and FB stack of each limb should be designed to sustain the rated pole-to-pole DC voltage of the HV side when a DC short circuit fault happens at the LV side. This sacrifices the overall system efficiency. It worth emphasizing that the DC transformers in [17] are applicable to asymmetrical monopole systems.

Therefore, this work extends the idea of DC auto-transformer suggested in [19] to generic MPCs capable of generating several AC and DC outputs from a fixed or variable AC or DC voltage. The proposed MPC provides a economical solution for a hybrid hub capable of facilitating: DC voltage and power control in complex DC grids. The basics of the presented MPC is described using two and three-port converters, and validated using simulation and experimental results. Also, this work clarifies the mathematical expressions that determine the AC and DC powers of the MPC, further than that explained in [19]. For instance, in the two-port converter, the AC power of the SC_2 determines the current stresses in the switches of the SC_2, not the entire DC power of the SC_2 as described in[19]. Moreover, it is found that the MPC with large number of ports facilitates better sharing of the power between the sub-converters; thus, decreases the rated power of the sub-converters and their current ratings.

II. MULTI-PORT CONVERTERS

Fig. 1 presents a number of MPCs capable of operating simultaneously as DC/DC and DC/AC converters in medium and high voltage DC and smart grids to control power and DC voltage, including DC voltage matching and tapping. The presented MPCs evolve from the DC transformers proposed in [19], and these MPCs were developed to facilitate large-scale integration of renewable power generations such as photovoltaic into MVDC and HVDC grids. The current stresses in the switches of the upper and lower sub-converters (SC_1 and SC_2) of the two-ports in Fig. 1 (a) vary with the power flow direction and DC voltage ratio. However, the current stresses in the switches of SCs decrease as the number of ports increases. Assuming the power flow and DC current directions shown in Fig. 1 (a) to be positive, the active powers that the SC1 and SC2 exchange with the AC side can be expressed as:

$$\begin{aligned} P_{ac1} &= \tfrac{3}{2} V_{m1} I_{m1} \cos(\delta_1 + \varphi_1) \approx 3(V_{dc1} - V_{dc2}) I_{d1} \\ P_{ac2} &= \tfrac{3}{2} V_{m2} I_{m2} \cos(\delta_2 + \varphi_2) \approx 3 V_{dc2} I_{d2} \end{aligned} \quad (1)$$

where, I_{d1} and I_{d2} are DC currents in the SC_1 and SC_2 arms ($I_{d1}=⅓I_{dc1}$ and $I_{dc2}=3(I_{d2}-I_{d1})\approx 3I_{d2}-I_{dc1}$, δ_1 and δ_2 are the voltage angles of the SC_1 and SC_2; φ_1 and φ_1 are phase shift between the grid voltage and currents of the SC_1 and SC_2; and V_{m1} and V_{m2}, and I_{m1} and I_{m2} are the peaks of the AC voltages and phase currents that the SC_1 and SC_2 present to interfacing transformers and inject into AC grid. It is worth emphasizing that I_{dc2} signifies the mismatch between I_{d1} and I_{d2} of the SC_1 and SC_2 should the circulating currents in their arms are well suppressed. On the other hand, P_{ac1} is stated as:

$$P_{ac1} = V_{dc1} I_{dc1} (1 - V_{dc2}/V_{dc1}) = P_{dc1}(n-1)/n \quad (2)$$

where, $n=V_{dc1}/V_{dc2}$ and $P_{dc1}=V_{dc1}I_{dc1}$. The total power transfer between the ac grid and SC_1 and SC_2 shown in Fig. 1 (a P_g represents the algebraic sum, i.e., $P_g=P_{ac1}+P_{ac2}$. The peak phase voltages at the AC terminals of the SC_1 and SC_2 are:

$$V_{m1}=½m_1(V_{dc1}-V_{dc2}) \quad (3)$$

$$V_{m2}=½m_2V_{dc2} \quad (4)$$

The current components related with the active power exchange between the AC and DC sides of the SC_1 and SC_2 are: $\frac{3}{4} m_1 I_{m1} \cos(\delta_1 + \varphi_1) \approx |I_{dc1}|$ and $\frac{3}{4} m_2 I_{m2} \cos(\delta + \varphi) \approx 3|I_{d2}|$.

When the power flow directions in the SC1 and SC2 are from AC to DC side (or from the DC to AC side), the transformer windings and switching devices of the SC_2 experience higher currents s than that of the SC1.

$$I_{d1}=⅓|I_{dc1}| \quad (5)$$

$$I_{d2}=⅓|I_{dc1}|+⅓|I_{dc2}| \quad (6)$$

If the polarity of the power flow in SC_1 is opposite to the polarity of the power flow in SC2, the average DC currents in the arms of the SC_1 and SC2 could be approximated by $I_{d1}=⅓|I_{dc1}|$ and $I_{d2}=⅓|I_{dc1}|-⅓|I_{dc2}|$, and the magnitudes of the AC current components associated with active powers in the transformer windings of the SC_1 and SC_2 can be expressed by:

$$|I_{dc1}| \approx \tfrac{3}{4} m_1 I_{m1} \cos(\delta_1 + \varphi_1) \quad (7)$$

$$\big||I_{dc1}| - |I_{dc2}|\big| \approx \tfrac{3}{4} m_2 I_{m2} \cos(\delta + \varphi) . \quad (8)$$

On other hand, the expression (8) and above discussions reveal that the switches and transformer windings connected to SC_2 will be exposed to reduced currents when the power flows in SC_1 and SC_2 are in the opposite directions. In this scenario, the power transfer between SC_1 and SC_2 via the AC side is:

$$V_{dc2}||I_{dc1}|-|I_{dc2}|| \quad (9)$$

When AC and DC sides of the MPC in Fig. 1 (a) are attached to AC and DC grids, AC powers P_{ac1} and P_{ac2} can be regulated to curb the current magnitudes in SC_1 and SC_2, independent of n. The reason is that P_{ac1} specifies the DC power to be transferred between the SC_1 and SC_2 through their arms, while bypassing the AC side:

$$P_{dc12}\approx P_{dc1}/n\approx P_{ac1}/(n-1) \quad (10)$$

Whilst P_{ac2} specifies the magnitudes of P_{dc2} to be transferred or provided from the AC side, and currents in the SC_2. In this way, the total DC power of the SC_2 (P_{dc2}) can be sourced via the arms of SC_1 and SC_2, with $P_{ac2}=0$ and zero currents on its semiconductor switches of SC_2, provided that the ratio n is adequately high to avoid overloading the switches of the SC_1.

Fig. 1 (b) presents an illustrative example of MPC that can synthesize several DC voltages, while ensuring that the currents are well-distributed between sub-converters. In the MPC in Fig. 1 (b), the SC_1 and SC_2 transfer power between their AC and DC sides using the same operating principle of the two-port converter explained earlier. Whilst SC_3 exchanges power via its AC link only, sharing an AC power (P_{ac1}) that the SC_1 presents to its AC side with SC_2. Such configuration decreases currents in the SC_2 when the three-port converter operates as an auto DC transformer. In this case, when the SC_1 is sourcing AC power (P_{ac1}) and SC_2 and SC_3 are both sinking AC powers P_{ac2} and P_{ac3}, the amount of AC power to be transferred through SC_2 is:

$$P_{ac2}=P_{ac1}-P_{ac3} \quad (11)$$

Therefore, setting P_{ac1} is enough for full definition of of the total DC power (P_{dc1}) at high-voltage DC terminal $P_{dc1}=nP_{ac1}(n-1)$, and the magnitude of DC power to be transferred between sub-converters 1 and 2, without passing via the AC side (P_{dc1}/n).

When AC side of the three-port converter is attached to the AC grid, the DC power (P_{dc2}) of sub-converter 2 is defined by P_{ac1} and P_{ac2}, with P_{ac1} defining the power transfer from sub-converter 1 to 2 via the DC side, without passing by the AC side, and P_{ac2} defines the power transfer from AC side of sub-converter 2 to its DC side:

$$P_{dc2}\approx P_{dc1}/n+P_{ac2}\approx P_{ac1}/(n-1)+P_{ac2} \quad (12)$$

In both of the above cases, the DC power of SC_3 (P_{dc3}) is determined exclusively by its AC power (P_{ac3}).

In addition to the above discussions, the MPCs in Fig. 1 could be realized by employing different topologies such as two-level converter[23], HB-MMC, FB-MMC and mixed cell MMC in SC_1, SC_2 and SC_3. For an example, when the MPC is employed for integration of medium-scale solar power plant that operates at MVDC into HVDC grid, the use of two-level converter in SC_3 could be justified. In similar way, other converter topologies could be employed in the SCs of the MPCs to deliver bespoke features.

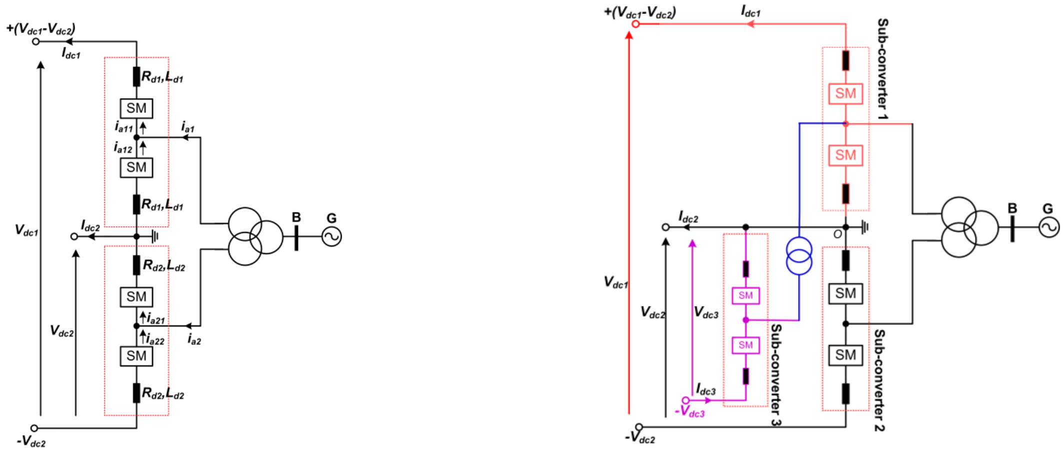

(a)

(b)

Fig. 1: Possible configurations of proposed MPCs: (a) Two-port converter and (b) Three-port converter

III. CONTROL SYSTEMS

When the AC side of the MPC is connected to AC grid as shown in Fig. 1 (a), the power transfer between its AC and DC terminals are controlled by varying the phase and magnitude of the voltage vectors at the AC terminals of the SC_1 and SC_2 relative to AC that of the AC grid. The angle difference δ_1-δ_2 contributes to definition of the magnitude and direction of the power P_{ac2} to be exchanged between the SC_1 and SC_2 via the AC side, and with the $I_{dc1}V_{dc2}=I_{dc1}V_{dc1}/n=P_{dc1}/n$ defines the DC power that the SC_1 and SC_2 exchange without passing via the AC side. When $\delta_1+\delta_2=0$, the net power injected into AC grid is zero; and this means the total AC power of the SC_1 is transferred to the SC_2 ($P_{ac2}=-P_{ac1}$, where $P_{ac1}=P_{dc1}(n-1)/n$ and $I_{dc2}=nI_{dc1}$), resembling the DC auto-transformer operation discussed earlier. When δ_2-$\delta_1=0$, zero power will be exchanged between the SC_1 and SC_2 via the AC side; instead, the total AC powers of the SC_1 and SC_2 will be transferred to AC grid, but this does not preclude power transfer through the DC side. The above discussions show that the sub-converters of the MPC based MMC can be controlled independently. When the AC side of the two-port converter is attached to an AC island with no generation (passive load), one of the sub-converters must regulate AC voltage in the AC link and the other sub-converter can control active power or DC voltage. Recall that setting P_{ac1} is enough for definition of the DC power at the HV DC terminal, $P_{dc1}=nP_{ac1}/(n-1)$ and DC link current $I_{dc1}=P_{dc1}/V_{dc1}=n/(n-1)\times P_{ac1}/V_{dc1}$.

When the SC1 and SC2 have opposite power flow directions and $P_{ac1}>P_{ac2}$, P_{ac2} defines the power transfer between the SC_1 and SC2 via the AC side and the power will be fed to the AC grid, $P_g=P_{ac1}+P_{ac2}$. Reconsidering the above scenario, but this time with $P_{ac2}>P_{ac1}$, P_{ac1} defines the power transfer between the SC1 and SC2 via the AC side and the power to be fed to the AC grid $|P_{ac1}-P_{ac2}|$. When the power flow directions in the SC_1 and SC_2 are in the same direction, no power will be exchanged between the SC_1 and SC_2 via the AC side; instead the whole power transfer will be via the DC side, and individual sub-converters and the AC grid. Considering a three-winding transformer model, the SC_1 and SC_2 of the two-port converter can be described with reference to the secondary and tertiary sides as:

$$\begin{aligned} L_{T1}\,di_{abc1}/dt + R_{T1}i_{abc1} &= v^{s}_{abcg} - \tfrac{1}{2}(V_{dc1}-V_{dc2}) - \tfrac{1}{2}(v_{labc1}-v_{uabc1}) \\ L_{T2}\,di_{abc2}/dt + R_{T2}i_{abc2} &= v^{t}_{abcg} - \tfrac{1}{2}V_{dc2} - \tfrac{1}{2}(v_{labc2}-v_{uabc2}) \end{aligned} \qquad (13)$$

where $R_{T1}=½R_{d1}+R_s+R_{ps}$ and $R_{T2}=½R_{d2}+R_t+R_{pt}$ and $L_{T1}=½L_{d1}+L_s+L_{ps}$ and $L_{T2}=½L_{d2}+L_t+L_{pt}$ stand for the transformer resistances and inductances referred to the secondary and tertiary sides; R_{ps} and R_{pt}, and L_{ps} and L_{pt} stand for the resistance and inductance of the primary windings referred to secondary and tertiary sides; R_s and R_t, and L_s and L_t are resistances and inductances of the secondary and secondary windings. Because of the asymmetrical nature of the SC_1 and SC_2 in Fig. 1 (a), the DC components $½(V_{dc1}-V_{dc2})$ and $½V_{dc2}$ cancel with those in the converters' terminal voltages v^{s}_{abcg} and v^{t}_{abcg} when seen from secondary and tertiary sides of the SC_1 and SC_2. Thus, $v^{s}_{abcg}-\frac{1}{2}(V_{dc1}-V_{dc2})\approx v_{abcs}$ and $v^{t}_{abcg}-\frac{1}{2}V_{dc2}\approx v_{abct}$, and since the DC free terminal voltages of the SC_1 and SC_2 can be expressed in terms of their corresponding upper lower arm voltages: $\frac{1}{2}(v_{labc1}-v_{uabc1})\approx v^{abc}_{c1}$ and $\frac{1}{2}(v_{labc2}-v_{uabc2})\approx v^{abc}_{c2}$. With these assumptions, (13) is transformed into d-q as:

$$\begin{aligned} di_{dq1}/dt &= -R_{T1}i_{dq1}/L_{T1} + (v_{dqs}-v_{cdq1}-j\omega L_{T1}i_{dq1})/L_{T1} \\ di_{dq2}/dt &= -R_{T2}i_{dq2}/L_{T2} + (v_{dqt}-v_{cdq2}-j\omega L_{T2}i_{dq2})/L_{T2} \end{aligned} \qquad (14)$$

Equation (14) indicates that two independent current controllers are needed for the SC_1 and SC_2 of the two-port converter in Fig. 1 Fig. 1(a). The current controllers to be incorporated into SC_1 and SC_2 can be expressed as:

$$\begin{aligned} \lambda_{dq1} &= k_{pi1}(i^{*}_{dq1}-i_{dq1}) + k_{ii1}\int(i^{*}_{dq1}-i_{dq1})dt \\ \lambda_{dq2} &= k_{pi2}(i^{*}_{dq2}-i_{dq2}) + k_{ii2}\int(i^{*}_{dq2}-i_{dq3})dt \end{aligned} \qquad (15)$$

$$\begin{aligned} v_{cdq1} &= v_{dqs} - j\omega L_{T1}i_{dq1} - \lambda_{dq1} \\ v_{cdq2} &= v_{dqt} - j\omega L_{T2}i_{dq2} - \lambda_{dq2} \end{aligned} \qquad (16)$$

Therefore, the outer controllers that regulate d-axis voltage in case of islanding operation, or active power or DC voltage in case of grid connection, define i^{*}_{d1} and i^{*}_{d2}, while i^{*}_{q1} and i^{*}_{q2} are defined from the outer controllers that regulate reactive power or AC voltage in grid connection case or q-axis voltage in case of islanding. The complete control systems used to regulate SC_1 and SC_2 of the MPCs being studied here are similar to the conventional power or DC voltage controlling converters of the modular converter based HVDC transmission systems. Also, a proportional-integral circulating current controller is implemented in each SC to suppress the 2nd and 4th harmonic currents in the MMC arms.

IV. SIMULATIONS

This section demonstrates the control flexibility of the multi-port DC-DC and DC-AC in Fig. 1. Each -converter is modelled an average MMC model. The system simulation parameters are:

arm reactors ($R_{d1}=R_{d2}$=0.5Ω, R_{d3}=0.4Ω; $L_{d1}=L_{d2}$=45mH and L_{d3}=30mH); cell capacitances ($C_{m1}=C_{m2}$=10mF and C_{m3}=8mF); interfacing transformer ($R_p=R_s=R_t$=0.002pu, $L_p=L_s=L_t$=0.05pu, 1300 MVA and 400 kV/300 kV/300 kV); and 400kV AC grid with 15000MVA three-phase short circuit fault level and X/R=15. In this demonstration, the SCs of the MPCs in Fig. 1 employs DC voltage, active power and reactive power controllers in the outer load; inner fundamental current control in synchronous reference frame; and a controller for circulating current suppression. The overall model (power circuit and control systems) is implemented in Matlab-Simulink.

A) Two-port converter

1) Four quadrant operation:

Fig. 2 displays simulation waveforms that illustrate the active powers exchange between the SC_1 and SC_2 of the two-port system being studied and AC grid. System operating conditions are summarised as follows:

- During interval $0 \le t < 0.8s$, the SC_1 is instructed to control its active power exchange with the AC grid at -390MW (negative sign entails the power flow direction is from AC to DC).
- At t=0.8s, SC_1 varies and reverses its power flow exchange with the AC grid to be -390MW to 650MW.
- During interval $0 \le t < 1.6s$, the SC_2 controls its output active power exchange with the AC grid at 390 MW (direction from DC to AC).
- At t=1.6s, SC_2 reverses its active power flow from 390MW to -650MW.

Fig. 2 (a) shows active power contribution of the SC_1 and SC_2, and the total active power the MPC exchanges with the AC grid. Observe that when the MPC exchanges zero power with AC grid, the SC_1 and SC_2 have the same power magnitude but with opposite polarities. This means that under this operating condition, the MPC in Fig. 1 (b) operates as the auto DC transformer proposed in [19]. Fig. 2 (b) displays the DC powers of the SC_1 and SC_2 and that being exchanged at the HV and LV DC terminals of the MPC. Fig. 2 (c) shows the DC currents in the SC_1 and SC_2 arms, and in the DC terminals of the HV and LV sides. Notice that although a large DC current is observed in the LV DC terminal, no sub-converter is exposed to excessive current stress.

2)Power control between DC terminals when AC terminal is connected to a passive load:

This section displays simulation waveforms when MPC in Fig. 1 (a) operates from a symmetrical DC link voltage of ±600kV, with its AC side connected to passive load. The passive load connected to ac side is 200MW and 50MVAr, and the secondary and tertiary windings of the 3-winding transformer are connected to the SC_1 and SC_2. The SC_1 is operated in an islanding mode that sets stiff AC voltage across the passive load, and the SC_2 locks to the AC voltage established by the SC_1 and controls active power as explained earlier. In time interval $0 \le t < 0.6s$, the SC_2 controls its active power P_{ac2} at zero. At t=0.6s, it increases P_{ac2} from 0 to 380 MW. (a) displays the active powers of the SC_1 and SC_2 P_{ac1} and P_{ac2}, and the power consumed in the AC island (passive AC load). Fig.3 (b) presents the DC powers being exchanged between the SC_1 and SC_2, including that in the LV and HV DC terminals. Fig.3 (c) presents DC components of the arm currents of the SC_1 and SC_2, and the DC currents in the LV and HV DC terminals. Notice that when the SC_2 controls its active power at zero, zero currents are seen in its arms, and in this period $I_{dc2}=-I_{dc1}$; thus $I_{d2}=0$, $P_{dc}(upper)=P_{dc}(lower)$, see Fig.3 (a) to (c). The results in Fig.3 demonstrate the increased control flexibility of the MPC when its AC side is connected to passive AC network with no generation.

B) Three-port converter

Fig.4 displays simulation traces for the three-port converter in Fig. 1 (b), with the power set-points of the sub-converters 1, 2 and 3 are P_{ac1}=-650 MW, P_{ac2}=325 MW and P_{ac}=325 MW. At t=0.8s, 1.6s and 2s, sub-converters 1, 2 and 3 have varied their set-points from -650MW to +1040MW, 325MW to -325MW and 325MW to -455MW respectively. Fig.4 (a) shows that in the time interval t<0.8s, the MPC in Fig. 1 Fig. 1(b) operates as a typical auto DC-transformer with multiple DC outputs and zero active power injection into the AC grid. Fig.4 (b) shows the DC powers at different DC terminals, including at SC_1. Fig.4 (a) and (b) confirm that the power distributions in the three-port converter obey to the same fundamentals as the two-port converter, i.e., $P_{ac1}=(n-1)/nP_{dc1}$ and $P_g=P_{ac1}+P_{ac2}+P_{ac3}$. It worth emphasizing that even though the DC power of SC_2 changes at $t=0.8s$ with P_{ac1} (as a results of internal DC power transfer via the DC side), the currents in the arms of sub-converter 2 remain to be distinctly determined by P_{ac2}, see Fig.4 (a), (b) and (c). Whilst the DC power and currents of the SC_3 are purely defined by P_{ac3}. Fig.4 (c) shows that the DC link currents and DC components of the arm currents of the different sub-converters and their distributions in SC_1 and SC_2 obey the same principles has been established for the two-port converter discussed in sections III and IV-A.

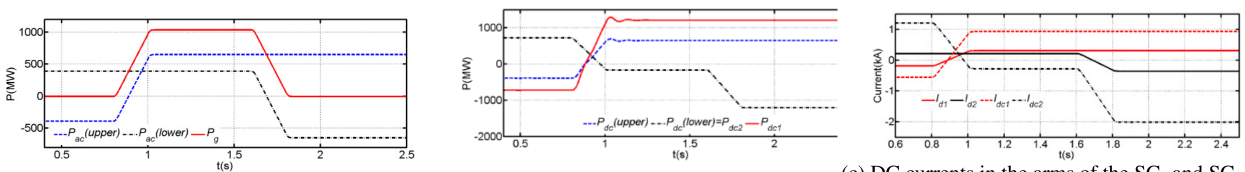

(a) $P_{ac}(upper)$ and $P_{ac}(lower)$, and AC power being exchanged with the AC grid, P_g

(b) $P_{dc}(upper)$ and $P_{dc}(lower)$, and DC power at HV and LV DC terminals, P_{dc1} and P_{dc2}

(c) DC currents in the arms of the SC_1 and SC_2, I_{d1} and I_{d2}, and in the HV and LV DC terminals, I_{dc1} and I_{dc2}

Fig. 2: Illustration of power control flexibility of the two-port converter when its HV and LV DC terminals are fed from active DC networks (V_{dc1}=1300 kV and V_{dc2}=600 kV) and its AC side is attached to AC grid: (a)

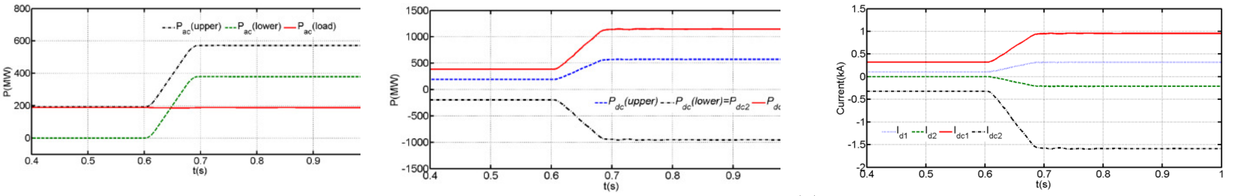

(a) Active powers of SC_1 and SC_2, P_{ac}(upper) and P_{ac}(lower), and active power being consumed by the AC load

(b) DC powers of SC_1 and SC_2, P_{dc}(upper) and P_{dc}(lower), and in the HV and LV DC terminals

(c) DC currents in the arms of the SC_1 and SC_2, I_{d1} and I_{d2}, and in the HV and LV DC terminals

Fig. 3: Illustration of power control when the proposed MPC converter is fed from a symmetrical DC bus of ±600kV, with its AC side is attached to passive load.

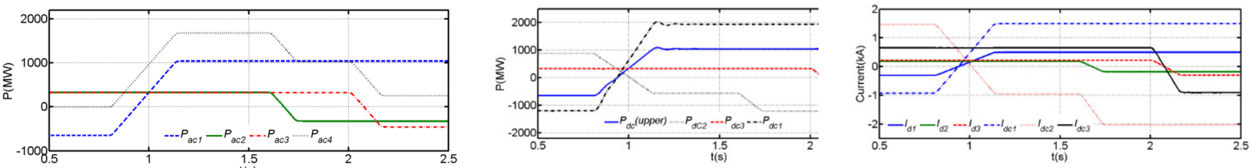

(a) Active powers of SC_1, SC_2 and SC_3, and total active exchange with the AC grid

(b) DC powers of SC_1, SC_2 and SC_3

(c) DC currents in the arms of SC_1, SC_2 and SC_3 and in their DC busses

Fig. 4: Illustrating of the power control in three-port converter when all its DC terminals are connected to active DC networks, with V_{dc1}=1300 kV, V_{dc2}=600 kV and V_{dc3}=500 kV, and its AC side is connected AC grid.

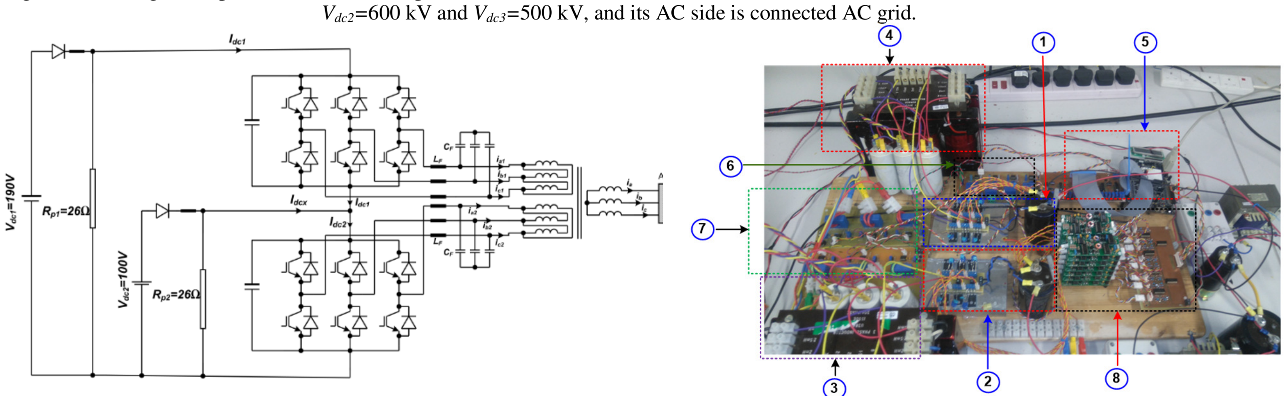

(a)

(b)

Fig. 5. (a) and (b) are details of the prototype (diagram and photo) when the SC_1 and SC_2 are realised by the conventional two-level converters:, with 1 and 2 signify SC1 and SC2; 3 and 4 signify AC filters of the SC_1 and SC_2; 5 is a microcontroller employed to program PWM and control systems; 6 and 7 are voltage and current senors; and 8 depicts the gate-drives and circuity that generates complementary PWM signal.

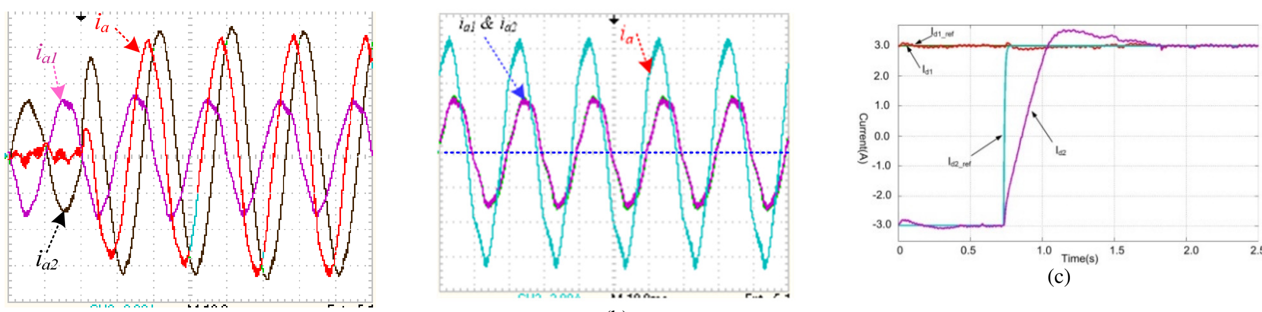

(a)

(b)

(c)

Fig. 6: Experimental demonstartion of the control flexibility of MPC converter when q-axis current orders of the SC_1 and SC_2 are held at zero (i_{q1}=i_{q2}=0). and i_{d1}=3A and step change is applied to i_{d2} from -3A to -3A:
(a) represents snapshot of the (i_{a1}, i_{a2} and i_a) zoomed around the time of application of step change to i_{d2} and (b) is the snapshot of the (i_{a1}, i_{a2} and i_a) when the system has reached the steady-state condition, (c) represents the direct axis currents of the SC_1 and SC_2 for the latter case. In both cases, the scales are maintained at (10ms/div and 2A/div)

V. EXPERIMENTAL VALIDATION

This section presents experimental validation of the theoretical discussions and simulation results of the MPC presented in sections II and IV using experimental results obtained from the scaled-down prototype of the two-port converter in Fig.5 (a) and (b). Although all the previous discussions assume that the SC_1 and SC_2 of the MPC are MMCs, the experimental prototype realizes these sub-converters by the two-level voltage source converters in Fig.5 (a) and (b). To realize bidirectional power flow using single-quadrant DC power supplies, a diode and an inductor and resistances R_{p1} and R_{p2} are added as shown in Fig.5 (a). The resistances are selected to ensure that the inequalities $I_{dc1}R_{p1}<V_{dc1}$ and $I_{dcx}R_{p2}<V_{dc2}$ are satisfied under all operating conditions. In this way, V_{dc1} and V_{dc2} remain virtually constant at 190V and 100V as the SC_1 and SC_2 vary their current set-points. Table I shows parameters of the prototype.

Table I: Test rig parameters

Parameter	Value
Grid voltage	45Vrms at 50Hz
dc voltage of the HV side (V_{dc1})	190V
dc voltage of the LV side (V_{dc2})	100V
ac side filtering inductance (L_F)	2.6mH
ac filtering capacitance (C_F)	30μF
Transformer voltage ratio	400/415/415
Carrier frequency	2.4kHz
DC link capacitances of SC1 and SC2	2.2mF

A)-Control flexibility

Fig.6 displays experimental waveforms of the two-port converter in Fig.6 when its operating conditions as follows: SC_1 regulates its d and q axis currents at $i_{d1}=3A$ and $i_{q1}=0$; and SC_2 varies its d-axis current i_{d2} from -3A to 3A, and its q-axis current is controlled at zero ($i_{q2}=0$).

Fig.6 (a) and (b) show phase 'a' currents of the SC_1 and SC_2 (black and purple) and total current being injected into AC grid (in red). Fig.6 (c) displays the d-axis currents of the SC_1 and SC_2 overlaid on their respective reference currents. Notice that the phase currents and their d-q components follow the current commands given to the SC_1 and SC_2, with zero grid current is observed when $i_{d2}=-i_{d1}$. This point out that under such operating condition, the MPC in Fig.5 operates as an auto DC-transformer described in [19].

VI. CONCLUSIONS

This paper has investigated several MPCs capable of operating as DC-DC and DC-AC converters and offer multiple DC and AC terminals. Detailed discussions of the presented MPCs demonstrate their suability for control of power and DC voltage, and DC voltage matching and tapping in complex medium and high-voltage DC grids. Comprehensive discussions, simulations and experimental waveforms have confirmed the enhanced control flexibility of the presented MPC, which is vital for resolving several outstanding control issues in future DC grids.

VII. ACKNOWLEDGMENT:

This project was funded by the Deanship of Scientific Research (DSR) at King Abdulaziz University, Jeddah, under grant no. (RG-5-135-38). The authors, therefore, acknowledge with thanks DSR For technical and financial support.

VIII. REFERENCES

[1] M. O. Khan, "Analyzing the effects of converter and DC line outages due to Distributed Voltage Control in AC-MTDC Distribution Network " *International Journal of Renewable Energy Research-IJRER,* vol. 8, no. 8, pp. 1740-1748, 2018.

[2] G. P. Adam, K. H. Ahmed, D. Holliday, S. J. Finney, G. M. Burt, and B. W. Williams, "Controlled transition bridge multilevel converter," in *2016 IEEE International Conference on Renewable Energy Research and Applications (ICRERA)*, 2016, pp. 794-798.

[3] G. P. Adam, K. H. Ahmed, and B. W. Williams, "Hybrid multilevel converter with dc side H-bridge chain links," in *Renewable Energy Research and Applications (ICRERA), 2013 International Conference on*, 2013, pp. 1002-1006.

[4] G. P. Adam, S. J. Finney, and B. W. Williams, "Enhanced control strategy of full-bridge modular multilevel converter," in *2015 International Conference on Renewable Energy Research and Applications (ICRERA)*, 2015, pp. 1432-1436.

[5] A. M. Omran, K. H. Ahmed, M. S. Hamad, and I. F. Al-Arabawy, "Interconnection between different DC technologies at multi-terminal HVDC network," in *Renewable Energy Research and Application (ICRERA), 2014 International Conference on*, 2014, pp. 295-300.

[6] K. Rouzbehi, Z. Jiebei, Z. Weiyi, G. B. Gharehpetian, A. Luna, and P. Rodriguez, "Generalized voltage droop control with inertia mimicry capability - step towards automation of multi-terminal HVDC grids," in *2015 International Conference on Renewable Energy Research and Applications (ICRERA)*, 2015, pp. 1556-1561.

[7] S. Li, F. Xingang, E. Alonso, M. Fairbank, and D. C. Wunsch, "Neural-network based vector control of VSCHVDC transmission systems," in *2015 International Conference on Renewable Energy Research and Applications (ICRERA)*, 2015, pp. 173-180.

[8] A. A. J. Far, M. Hajian, D. Jovcic, and Y. Audichya, "High-power modular multilevel converter optimal design for DC/DC converter applications," *IET Power Electronics,* vol. 9, no. 2, pp. 247-255, 2016.

[9] M. Corti, E. Tironi, and G. Ubezio, "DC Networks Including Multi-port DC/DC Converters: Fault Analysis," *IEEE Transactions on Industry Applications,* vol. PP, no. 99, pp. 1-1, 2016.

[10] R. Kondo, Y. Higaki, and M. Yamada, "Proposition and experimental verification of a bi-directional isolated DC/DC converter for battery charger-discharger of electric vehicle," in *2016 IEEE Applied Power Electronics Conference and Exposition (APEC)*, 2016, pp. 1713-1720.

[11] P. Gaur, N. Soren, and D. Bhowmik, "Impact Assessment of Vehicle-to-grid Technology in LFC of Multi-area Solar-thermal Power System," *International Journal of Renewable Energy Research-IJRER,* vol. 8, no. 3, pp. 1582-1590, 2018.

[12] M. Moazzami, J. Moradi, H. Shahinzadeh, G. B, Gharehpetian, and H. Mogoei, "Optimal Economic Operation of Microgrids Integrating Wind Farms and Advanced Rail Energy Storage System," *International Journal of Renewable Energy Research-IJRER,* vol. 8, no. 2, 2018.

[13] R. C, C. H. Basha, and S. odofin, "A Review on Non-isolated Inductor Coupled DC-DC Converter for Photovoltaic Grid-Connected Applications," vol. 7, no. 4, pp. 1571-1585, 2017.

[14] B. Zhao, Q. Song, J. Li, X. Xu, and W. Liu, "Comparative Analysis of Multilevel-High-Frequency-Link and Multilevel-DC-Link DC–DC Transformers Based on MMC and Dual-Active Bridge for MVDC Application," *IEEE Transactions on Power Electronics,* vol. 33, no. 3, pp. 2035-2049, 2018.

[15] P. Li, G. P. Adam, S. J. Finney, and D. Holliday, "Operation Analysis of Thyristor Based Front-to-Front Active-Forced-Commutated Bridge DC Transformer in LCC and VSC Hybrid HVDC Networks," *IEEE Journal of Emerging and Selected Topics in Power Electronics,* vol. PP, no. 99, pp. 1-1, 2017.

[16] D. Jovcic and H. Zhang, "Dual Channel Control With DC Fault Ride Through for MMC-Based, Isolated DC/DC Converter," *IEEE Transactions on Power Delivery,* vol. 32, no. 3, pp. 1574-1582, 2017.

[17] Y. Jie, H. Zhiyuan, P. Hui, and T. Guangfu, "The Hybrid-Cascaded DC–DC Converters Suitable for HVdc Applications," *Power Electronics, IEEE Transactions on,* vol. 30, no. 10, pp. 5358-5363, 2015.

[18] I. A. Gowaid, G. P. Adam, B. W. Williams, A. M. Massoud, and S. Ahmed, "The transition arm multilevel converter – A concept for medium and high voltage DC-DC transformers," in *2015 IEEE International Conference on Industrial Technology (ICIT)*, 2015, pp. 3099-3104.

[19] A. Schon and M. M. Bakran, "High power HVDC-DC converters for the interconnection of HVDC lines with different line topologies," in *Power Electronics Conference (IPEC-Hiroshima 2014 - ECCE-ASIA), 2014 International*, 2014, pp. 3255-3262.

[20] S. Kenzelmann, D. Dujic, F. Canales, Y. R. De Novaes, and A. Rufer, "Modular DC/DC converter: Comparison of modulation methods," in *Power Electronics and Motion Control Conference (EPE/PEMC), 2012 15th International*, 2012, pp. LS2a.1-1-LS2a.1-7.

[21] I. A. Gowaid, G. P. Adam, A. M. Massoud, S. Ahmed, D. Holliday, and B. W. Williams, "Quasi Two-Level Operation of Modular Multilevel Converter for Use in a High-Power DC Transformer With DC Fault Isolation Capability," *Power Electronics, IEEE Transactions on,* vol. 30, no. 1, pp. 108-123, 2015.

[22] I. A. Gowaid, G. P. Adam, A. M. Massoud, S. Ahmed, and B. W. Williams, "Hybrid and Modular Multilevel Converter Designs for Isolated HVDC–DC Converters," *IEEE Journal of Emerging and Selected Topics in Power Electronics,* vol. 6, no. 1, pp. 188-202, 2018.

[23] S. Ray, N. Gupta, and R. A. Gupta, "Prototype Development and Experimental Investigation on Cascaded Five-Level Inverter Based Active Filter for Large-Scale Grid-tied Photovoltaic" *International Journal of Renewable Energy Research-IJRER,* vol. 8, no. 3, pp. 1800-1811, 2018.